RSC Advances

PAPER

View Article Online
View Journal | View Issue

Cite this: *RSC Adv.*, 2025, **15**, 35047

Continuous microwave tunnel expansion of vermiculite: a comparative study with thermal/chemical methods for structure-intact performance enhancement

Yi-Wen Shen,[a] Jie Bian,[a] Yan-Bo Wang,[a] Xin-Yu Yang *[a] and Wei-Liang Tian*[ab]

Received 14th July 2025
Accepted 11th September 2025

DOI: 10.1039/d5ra05038c

rsc.li/rsc-advances

Vermiculite (VMT) expansion technology requires innovation to overcome its low efficiency and limited mechanical properties. Therefore, herein, a tunnel-type continuous microwave method was employed to optimize the VMT expansion process and enhance the performance and industrial value of the expanded VMT (EVMT). The microwave-expanded VMT (M-EVMT) exhibited minimal damage to the raw VMT structure compared with the thermal/chemical expansion methods, and at a 12 kW microwave power and 0.3 m min^{-1} conveyor belt speed, the raw VMT with 2.8–8 mm particle size could achieve larger interlayer microwave expansion and maintain its intact structure. Meanwhile, M-EVMT demonstrated unprecedented mechanical flexibility while maintaining a complete layered structure. This microwave method integrated mineral processing with circular economy, enhancing the energy efficiency, material performance, and industrial scalability of sustainable building materials.

Introduction

The research on process optimization, structural performance regulation, and industrial sustainability of microwave vermiculite (VMT) expansion technology in continuous tunnel systems has demonstrated significant potential in enhancing the production efficiency of expanded vermiculite (EVMT). VMT is a naturally formed layered aluminosilicate,[1,2] which has garnered considerable industrial interest due to its unique interlayer hydrodynamics and structural scalability. EVMT could be obtained by increasing the interlayer spacing of raw VMT through various methods.[3] The expansion mechanism is mainly driven by the instantaneous vaporization of the thermally excited interlayer water,[4] which not only controls the macroscopic expansion volume ratio (typically 8–30 times than the raw VMT) but also influences the evolution of the microstructure, thereby determining the final performance of the material.[5] Microwave, thermal, and chemical techniques are commonly used for raw VMT expansion to obtain microwave-expanded vermiculite (M-EVMT), thermally expanded vermiculite (T-EVMT) and chemically expanded vermiculite (C-EVMT), respectively. In terms of process optimization, microwave heating is more energy-efficient than traditional thermal and chemical methods,[6] with advantages such as faster heating, ease of operation, and effective reduction in environmental pollution. Additionally, adjusting the microwave power and radiation time can further optimize the expansion volume ratio and bulk density of the EVMT, respectively.[7]

EVMT exhibits exceptional functional characteristics, including low densities (60–150 kg m^{-3}), ultra-low thermal conductivities (0.05–0.07 W m^{-1} K^{-1}), and hierarchical porosities.[8] These properties make EVMT a strategic material in sustainable construction, environmental remediation and precision agriculture.[9–11] Despite these merits, industrial-scale EVMT production confronts three critical technological barriers: (1) energy-intensive thermal expansion (800–1200 °C) relying on fossil fuels results in inconsistent expansion and embrittlement;[12,13] (2) chemical expansion introduces corrosive agents that can harm the environment,[14] and the structural integrity and porosity of the expanded material could be affected, which in turn impacts its functional performance; and (3) microwave-assisted processes, while enabling rapid dielectric heating, suffer from discontinuous operation and suboptimal energy coupling in conventional cavity designs.[15] Thus, the uneven expansion and easy embrittlement of EVMT are still challenges.

To tackle these challenges, we engineered a continuous microwave tunnel expansion device. This device is designed to overcome the phase transitions that cause brittleness in conventional thermal processing and achieve continuous production of EVMT while simultaneously eliminating the need for chemical auxiliaries and improving the expansion uniformity and mechanical flexibility. This innovation achieves the

[a]*College of Chemistry and Chemical Engineering, Tarim University, Alar 843300, China. E-mail: xyyang_1995@163.com; twllong@126.com*

[b]*State Key Laboratory of Chemical Resource Engineering, College of Chemistry, Beijing University of Chemical Technology, Beijing, 100029, China*

efficient and uniform expansion of raw VMT using microwave energy for the first time, significantly enhancing the pore structure and adsorption performance of EVMT. It offers a novel approach to the development of green and environmentally friendly building materials.

Materials and methods

Materials and reagents

Five different sizes of raw vermiculite particles (0.3–1 mm, 1–1.5 mm, 0.71–2 mm, 1.4–4 mm, and 2.8–8 mm) were purchased from Xinjiang Yuli Xinlong Vermiculite Co., Ltd, which were cleaned and dried in an oven at 85 °C for 24 h before use. Hydrogen peroxide (H_2O_2) was bought from Xilong Science Co., Ltd (Sichuan, China).

Preparation of M-EVMT

The microwave-expanded vermiculite was synthesized using a continuous microwave tunnel expansion device (machine power: 18 kW, equipment model: DLW-12EMV-2X, factory serial number: DLW-230708, equipment dimensions: 6320 × 1220 × 220 mm, Dezhou Liwei Biotechnology Co., Ltd). The raw VMT was poured into the feeding port, and the conveyor belt and microwave radiation lamp were turned on. Finally, the M-EVMT particles were collected at the discharge port to analyze the expansion efficiency. The desired microwave power and conveyor belt speed were set on the system's control panel. The tested parameters of microwave power (kW) were 3, 6, 9 and 12, and the conveyor belt speed (m min^{-1}) was 0.3, 0.6, 0.9 and 1.2, respectively. The cavity length inside the microwave device was 2.4 m; thus, the actual microwave expansion time for raw VMT at the conveyor belt speeds of 0.3, 0.6, 0.9 and 1.2 m min^{-1} were 8, 4, 2.7 and 2 min, respectively.

Preparation of T-EVMT

The thermally expanded vermiculite was synthesized using a tube furnace (OTF-1200X, Hefei Kejing Materials Technology Co., Ltd), the tube furnace was heated at a rate of 10 °C min^{-1} to 800 °C, then, the raw VMT was placed in tube furnace and thermally expanded for 5 min, followed by cooling to room temperature to collect the final products.

Preparation of C-EVMT

In a 500 mL beaker, the raw VMT was immersed in 30 wt% H_2O_2 solution and placed in an oven at 65 °C; the C-EVMT could be obtained after a 24 h expansion.

Measurement and characterization techniques

X-Ray diffraction (XRD) patterns were recorded using a German Bruker D8 advance diffractometer (Cu Kα, 40 kV/40 mA, λ = 0.15418 nm, 0.1 step, 5–70°). Fourier-transform infrared (FTIR) spectra were recorded using a Thermo Scientific Nicolet iS50 infrared spectrometer, scanning over the range of 4000–400 cm^{-1}. The morphology of the samples was observed by a scanning electron microscope (SEM, Zeiss Supra 55, German). Thermogravimetry (TG, Netzsch STA 449 F3, German) was performed at a linear heating rate of 30 °C min^{-1} over the temperature range from room temperature to 1000 °C in an N_2 atmosphere. The bulk density of the EVMT was calculated using the formula: Bulk density (g mL^{-1}) = EVMT mass (g)/EVMT volume (mL). The volume ratio was calculated as follows: Volume ratio = V_1/V_0, where V_1 and V_0 are the volume (mL) of the expanded VMT and raw VMT, respectively.

Results and discussion

Fig. 1 clearly illustrates the expansion process of raw VMT using microwave, thermal and chemical expansion methods, along with the physical images of raw VMT, C-EVMT, M-EVMT and T-EVMT. The raw VMT is golden-brown, possesses a certain luster, and displays a clear flaky structure. After expansion, the layered structure of VMT becomes more distinct. Following the different expansion processes, all the obtained EVMTs have a "worm-like" multi-layer structure;[16] however, a notable color transformation is observed in them. The color of T-EVMT, M-EVMT and C-EVMT is gradually changed from yellow to white. T-EVMT prepared at a relatively high temperature causes the surface of T-EVMT to become slightly yellow. C-EVMT, which used the H_2O_2 agent for chemical expansion, has a slightly whitish coloration, accompanied by partial corrosion of the layered structure. Additionally, the obtained M-EVMT is further subjected to secondary thermal, microwave and chemical expansions, and the secondary expanded materials of M-T-EVMT, M-M-EVMT and M-C-EVMT are prepared. A comparative analysis reveals that secondary expansion yields superior results to primary expansion, as evidenced by the enhanced brightness and color saturation.

Fig. 2a shows the layered crystal structure of EVMT and the increased layer spacing of the raw VMT after expansion. The cross-sectional morphologies of EVMTs prepared using various methods are different, and the SEM images could clearly reveal the longitudinal expansion process. Fig. 2b–d are the SEM images of raw VMT, M-EVMT and M-M-EVMT, respectively, which clearly demonstrate that the layered structure is transformed from a tightly packed configuration in the raw VMT to an expanded state following a single microwave treatment, where the layers extend outward from the interior. After two microwave expansion treatments, the layered structure of M-M-EVMT is not damaged, and the interlayer spacing is further increased.[17] Fig. 2e–g are the SEM images of C-VMT, M-EVMT and T-EVMT, respectively. As shown in Fig. 2e, the use of H_2O_2 in chemical expansion could thicken the pore walls of C-EVMT; additionally, the solution residues result in an indistinct layered morphology and smaller interlayer pores.[18,19] As illustrated in Fig. 2f, M-EVMT exhibits essentially a uniform interlayer spacing, with minimal damage to the raw VMT structure. Furthermore, M-EVMT shows a more ordered layered structure.[20] As depicted in Fig. 2g, the cross-section of thermally expanded VMT at 800 °C presents a corrugated pattern, and the layers of T-EVMT are widely separated, forming a porous structure with more complete interlayer detachment. It is evident that M-EVMT and T-EVMT display more pronounced

Fig. 1 Preparation methods for EVMT.

and well-defined layered structures compared with C-EVMT,[21,22] which highlights the distinct morphological differences between raw VMT and EVMT. Meanwhile, M-EVMT demonstrates an unprecedented mechanical flexibility while maintaining a complete layered structure and equivalent expansion volume ratio, which can be seen in Movie S1 in the SI.

The XRD characterization results are presented in Fig. 3a–c. As shown in Fig. 3a, the characteristic peaks at 2θ of 8.8°, 26.7° and 45° correspond to the 003, 009 and 0015 crystallographic planes of raw VMT, respectively. In addition, the characteristic diffraction peak intensity gradually diminishes with the increasing particle size of raw VMT. This is probably because the larger particle size exhibits stronger van der Waals forces and hydrogen bonds, leading to easy agglomeration. The raw VMT particles within the agglomerates stack on top of each other, and some crystal planes are blocked, resulting in a reduction in the number of crystal planes actually participating in diffraction. Therefore, the characteristic peaks of the raw VMT with larger particle sizes are weakened.

As shown in Fig. 3b, the characteristic peaks of the raw VMT remain intact after microwave expansion, indicating that the structural integrity of the raw VMT is preserved,[23] which is consistent with the results observed by SEM. As shown in Fig. 3c, when the raw VMT is subjected to secondary microwave expansion, the main characteristic peaks of the raw VMT still exist in the prepared M-M-EVMT. This indicates that microwave radiation does not damage the structure of the raw VMT and is a mild expansion method, which effectively preserves the

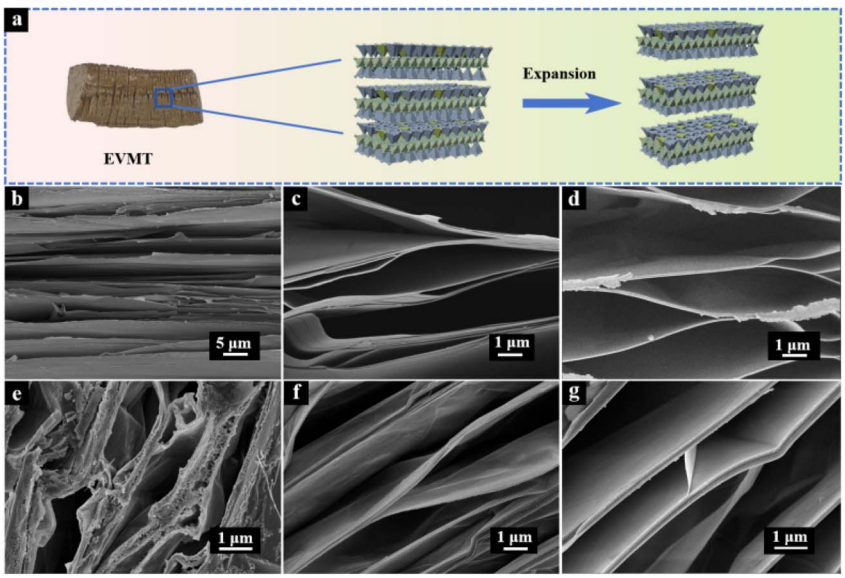

Fig. 2 (a) Crystal structure diagram of expanded VMT; (b) SEM image of raw VMT; (c) SEM image of M-EVMT; (d) SEM image of M-M-EVMT; (e) SEM image of C-EVMT; (f) SEM image of M-EVMT; and (g) SEM image of T-EVMT.

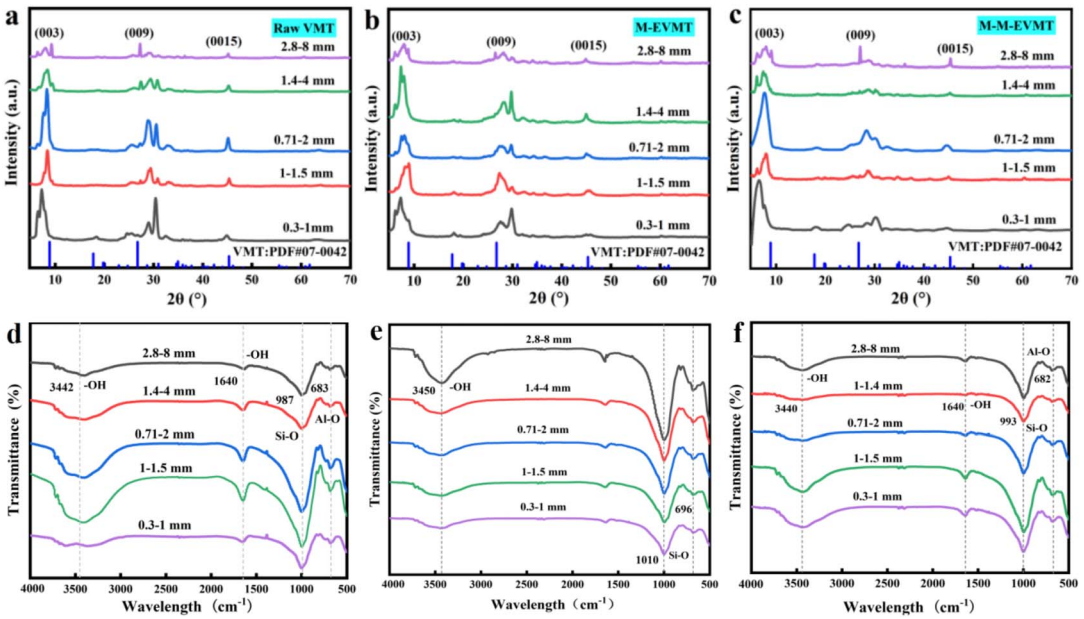

Fig. 3 XRD patterns of the raw VMT (a), M-EVMT (b), and M-M-EVMT (c). FTIR spectra of the raw VMT (d), M-EVMT (e), and M-M-EVMT (f) with different particle sizes.

internal structure of the raw VMT. By comparing the XRD patterns of the raw-VMT, M-EVMT and M-M-EVMT with the same particle size (0.3–1 mm), the influence of microwave expansion on the interlayer spacing of VMT is analyzed. The characteristic peak of the 003 crystallographic plane in raw VMT is 7.32°. After one round of microwave expansion, this characteristic peak shifts to 7.26°. Following a second round of microwave expansion, the characteristic peak further shifts to 6.54°, which indicates that as the expansion process proceeds, the diffraction angle of the 003 crystallographic plane shifts toward smaller angles, suggesting an increase in the interlayer spacing of the EVMTs.

During the microwave expansion process, the evaporation of water molecules between the layers of VMT and the reorganization of the hydrogen bond networks have a significant impact on the structure of VMT. These changes are manifested in the infrared spectrum as shifts in the absorption peaks for the O–H stretching vibration, interlayer O–H bonds, Si–O–Si asymmetric stretching vibration and Al–O bonds. Fig. 3d shows the FTIR spectrum of the raw VMT. It has a relatively wide absorption peak near 3442 cm^{-1}, corresponding to the O–H stretching vibration formed by intramolecular hydrogen bonds.[24] The peak at 1640 cm^{-1} is attributed to the O–H bond present between the layers of VMT. The pronounced peak at 987 cm^{-1} is attributed to the asymmetric stretching vibration of Si–O–Si, while the peak near 683 cm^{-1} signifies the presence of an Al–O bond.[25] As shown in Fig. 3e, the peak corresponding to the O–H stretching vibration in M-EVMT is 3450 cm^{-1}, which is slightly shifted compared to that of the raw VMT (3442 cm^{-1}), indicating that there is a change in the hydrogen bonding environment due to the microwave expansion process. As shown in Fig. 3f, the O–H stretching vibration peak in M-M-EVMT is at 3440 cm^{-1}, which is different from both the raw VMT and M-EVMT, suggesting that the secondary microwave expansion process further modified the hydrogen bonding environment. In addition, the main characteristic peaks of the infrared spectra of the raw VMT, M-EVMT and M-M-EVMT with different particle sizes are basically the same, further indicating that microwave radiation does not damage the layered structure of VMT.

As shown in Fig. 4a, which is the FTIR spectra of M-EVMT under different microwave powers, with an increase in microwave radiation power from 3 to 12 kW, the main characteristic peaks are significantly enhanced, indicating that the higher the radiation power, the better the expansion efficiency. The FTIR spectra of M-EVMT under different conveyor belt rates are shown in Fig. 4b, which indicate that as the conveyor belt rate increases from 0.3 to 1.2 m min^{-1}, the characteristic peaks intensity of the M-EVMT gradually decreased, because the speed of the conveyor belt affects the radiation time that VMT stays in the microwave equipment. The slower the conveyor belt speed and the longer the microwave radiation time. Thus, the raw VMT exhibits optimal expansion and the strongest infrared characteristic peak at a conveyor belt speed of 0.3 m min^{-1}. As can be seen from Fig. 4c, with the increase in the raw VMT particle size, the expansion volume ratio increases. At a low microwave power of 3 kW, the expansion efficiency of VMT is very low, and the expansion volume ratio is the best at a high microwave power of 12 kW. A higher microwave power can achieve an extremely fast heating rate, causing the water between the VMT layers to overheat rapidly and vaporize intensely, thereby generating a higher instantaneous vapor pressure and more thorough opening up of its layered structure. As can be seen from Fig. 4d, the longer residence time of the material at a lower speed increases the microwave radiation time. Therefore, the optimal conveyor belt flow rate is 0.3 m min^{-1}, and when combined with a power of 12 kW, the

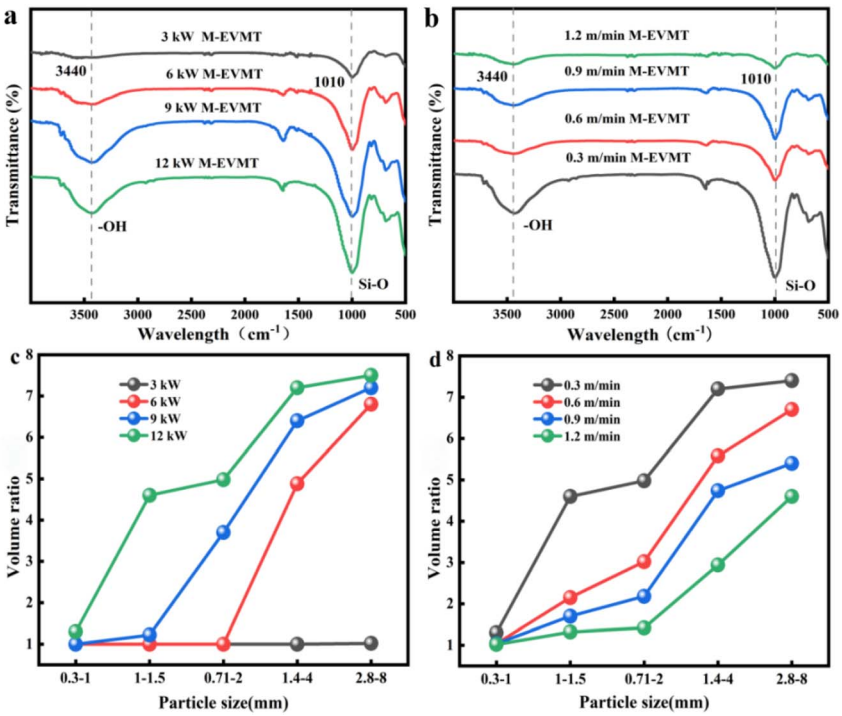

Fig. 4 (a) FTIR spectra of M-EVMT under different microwave radiation powers; (b) FTIR spectra of M-EVMT under different conveyor belt rates; (c) expansion volume ratio of M-EVMT with raw VMT under different microwave radiation powers (0.3 m min^{-1} conveyor belt rate); and (d) expansion volume ratio of M-EVMT with raw VMT under different conveyor belt rates (12 kW microwave radiation power).

highest expansion ratio of M-EVMT is achieved. The results of the experiment are consistent with those of the infrared analysis.

Fig. 5a is the volume ratio of C-EVMT to the raw VMT. In the chemical expansion method, the expanded volume ratio is closely related to the particle size. The experimental results show an upward trend as the particle size increases. The raw VMT with a particle size of 2.8–8 mm achieves the highest chemical expansion volume. Fig. 5b shows the volume ratio of T-EVMT to the raw VMT at different particle sizes. The variation trend aligns well with that observed in chemical expansion; as the particle size of the raw VMT increases, the expansion volume ratio also increases. Fig. 5c presents the expanded volume ratio with particle size during microwave expansion.

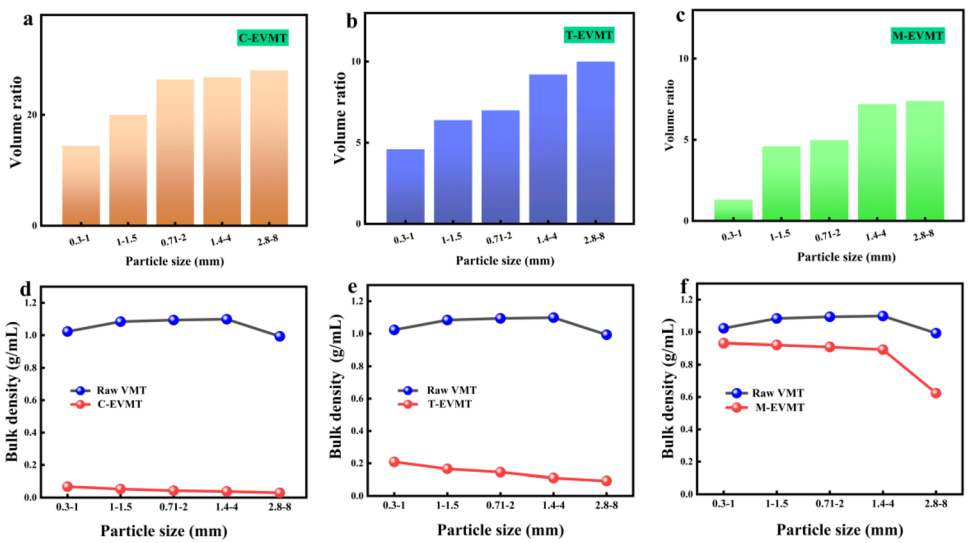

Fig. 5 (a) Volume ratio of C-EVMT to raw VMT; (b) volume ratio of T-EVMT to raw VMT; (c) volume ratio of M-EVMT to raw VMT (0.3 m min^{-1} conveyor belt rate and 12 kW radiation power); (d) bulk density of C-EVMT; (e) bulk density of T-EVMT; and (f) bulk density of M-EVMT.

Specifically, the raw VMT with a particle size of 0.3–1 mm exhibits the lowest expansion volume, while the raw VMT with a particle size of 0.28–8 mm achieves the highest expansion volume. Overall, the chemical expansion method results in a significantly larger volume increase than those of thermal and microwave expansions. Fig. 5d–f presents the bulk density of C-EVMT, T-EVMT and M-EVMT. It could be concluded that the bulk density of EVMT produced by different expansion methods has decreased compared with the raw VMT, and the bulk density of C-EVMT and T-EVMT obtained through chemical expansion and thermal expansion, respectively, is much lower than that of the raw VMT. In contrast, the microwave expansion shows minimal change in the bulk density, and the bulk density of M-EVMT is not obviously changed, indicating that the structure of VMT is not damaged during the microwave treatment, and the structural water between the layers of VMT can effectively maintain its original structure.[26] The microwave expansion method is convenient and quick, the expansion effect is comparable to that of thermal expansion, and continuous and uninterrupted production can be easily achieved, making it an efficient alternate way to obtain expanded VMT in industrial production.

The infrared spectra of C-EVMT with different particle sizes are presented in Fig. 6a. All the samples exhibited strong –OH stretching vibration peaks at 3440 cm^{-1}, indicating that EVMTs retained their interlayer water molecules after chemical expansion. Additionally, the characteristic peaks at 996 cm^{-1} (Si–O) and 703 cm^{-1} (Al–O) are clearly observed, demonstrating that the layered silicate structure remained largely intact. Fig. 6b shows the infrared spectra of T-EVMT with different particle sizes. The characteristic peaks of T-EVMT are basically consistent with those of the raw VMT. The peak intensity of T-EVMT with different particle sizes is basically the same, suggesting that the thermal expansion uniformly affected the structure. Fig. 6c shows the infrared spectra of the raw VMT, C-EVMT, T-EVMT and M-EVMT with particle sizes between 2.8 and 8 mm. The thermally expanded VMT loses more interlayer water molecules due to the high temperature; therefore, the –OH peak of T-EVMT near 3440 cm^{-1} is weaker, and the characteristic peak intensity of –OH in M-EVMT is the strongest, indicating that the number of water molecules in M-EVMT is the largest. Fig. 6d–f shows that C-EVMT, T-EVMT and M-EVMT exhibit similar thermal stability in the TG analysis. However, their weight loss rates at specific temperatures differ, which may be related to their preparation methods and physical properties.[27] Significant differences exist in the thermal behaviors of C-EVMT, M-EVMT and T-EVMT. The DTG curve of C-EVMT (Fig. 6d) exhibits two weight-loss peaks. The first peak occurs at 87.4 °C, corresponding to the removal of surface-adsorbed water and part of the interlayer water. The second peak at around400 °C may be attributed to the decomposition of residual chemical reagents or the oxidation of the interlayer organic components. The high total mass loss indicates that chemical treatment introduces a large number of volatile or decomposable components. The main weight-loss peak of the DTG curve of M-EVMT (Fig. 6e) is at 82.4 °C, corresponding to the rapid removal of interlayer water, which suggests that microwave treatment results in a more concentrated distribution of interlayer water. The peak at 947.4 °C may be related to the removal of structural hydroxyl groups and the decomposition of trace residues.[28,29] The DTG curve of T-EVMT (Fig. 6f) shows a broad weight-loss peak at 77.3 °C, reflecting a progressive dehydration process. The peaks at 762.3 and 937.3 °C correspond to the decomposition of hydroxyl groups from the VMT layer.

Based on the previous research results, under the conditions of 0.3 m min^{-1} conveyor belt rate and 12 kW radiation power, the volume ratio of M-EVMT to raw VMT is 7.4. Fig. 7 shows the change in the expansion volume when M-EVMT undergoes a secondary expansion process. The secondary expansion *via* microwave or thermal methods yields a volume ratio of 1, indicating minimal or no further expansion. In contrast, the M-

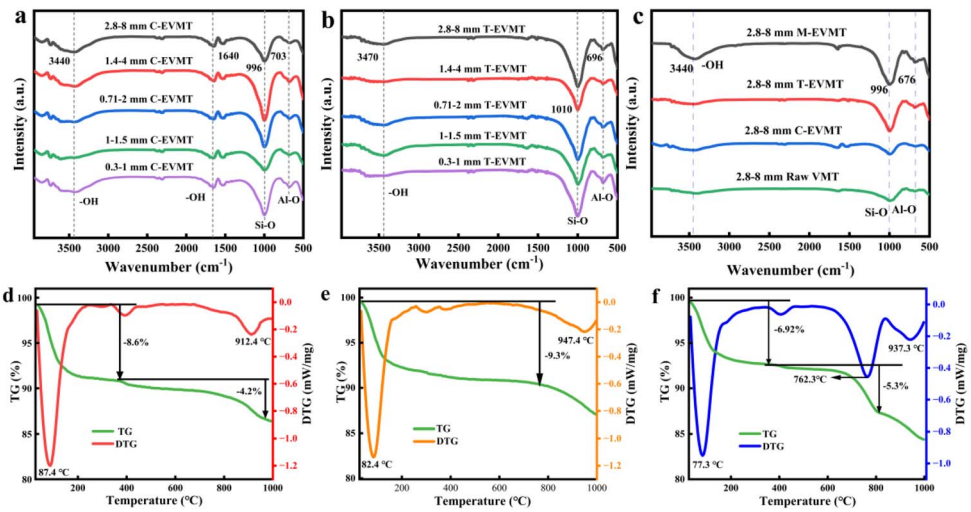

Fig. 6 (a) FTIR spectra of C-EVMT; (b) FTIR spectra of T-EVMT; (c) FTIR spectra of the raw VMT, C-EVMT, M-EVMT and T-EVMT (2.8–8 mm) and the corresponding TG-DSC curves of C-EVMT (d), T-EVMT (e), and M-EVMT (f).

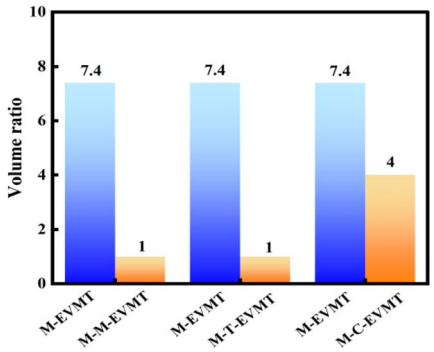

Fig. 7 Comparison of secondary expansion.

C-EVMT sample exhibits a secondary chemical expansion volume ratio of 4, demonstrating that chemical treatment enables significant additional expansion even after the initial microwave expansion. The decomposition of hydrogen peroxide generates water molecules and oxygen,[30] which promotes the renewed expansion of the VMT interlayers through the action of water vapor pressure.

Conclusions

This study optimized microwave-assisted VMT expansion parameters, revealing the structure–property relationships. The raw VMT was expanded by chemical, thermal and microwave expansion methods, which showed that the pore walls of C-EVMT became thicker due to the use of hydrogen peroxide for chemical expansion. M-EVMT obtained from microwave radiation exhibited minimal damage to the raw VMT and exhibited a more ordered layered structure. The cross-section of T-EVMT had a wide interlayer separation and indicated the formation of a porous structure. With the increase in the particle size of the raw VMT, the expansion volume increased. At low microwave powers, the expansion efficiency was very low. At higher microwave powers, an extremely fast heating rate could be achieved, generating a higher instantaneous vapor pressure and more thorough opening up of its layered structure. At low transmission speeds, VMT had a longer residence time, which increased the microwave radiation time. Under a 12 kW microwave power and 0.3 m min^{-1} conveyor belt speed, 2.8–8 mm particles achieved interlayer microwave expansion and maintained their intact structure. During secondary expansion, the volume of the thermally and chemically expanded VMT remained unchanged, whereas microwave-expanded VMT underwent further chemical expansion with an additional 4-fold volume increase. Our continuous tunnel microwave device effectively solves the intermittent mass fluctuations during VMT processing. This establishes a lab-to-industry transformation pathway for sustainable mineral manufacturing.

Conflicts of interest

The authors declare no conflicts of interest.

Data availability

All data generated or analyzed during this study are included in this published article.

Supplementary information is available. See DOI: https://doi.org/10.1039/d5ra05038c.

Acknowledgements

This work was supported by the Nanjiang Technology Project (2023AB028), Patent Transformation and Application and Industrialization Project (BTSCJGJ-ZSCQ-2024004), President's Fund Major Project Cultivation Special (TDZKZD202502), State Key Laboratory of Chemical Resource Engineering (CRUZD2301), and the presidential research fund of Tarim University (TDZKSS202127).

References

1 W. Xie, Y. Chen and H. Yang, Layered clay minerals in cancer therapy: recent progress and prospects, *Small*, 2023, **19**(34), 2300842.
2 P. F. Bergmann Becker, C. Effting and A. Schackow, Lightweight thermal insulating coating mortars with aerogel, EPS, and vermiculite for energy conservation in buildings, *Cem. Concr. Compos.*, 2022, **125**, 104283.
3 X. Zhang, H. You, J. Hou, Z. Li, Y. Feng, Y. Lin, X. Dai, K. Zhang and W. Tian, Green and scalable narrow-gap exfoliation of high-quality two-dimensional vermiculite nanosheets as poly (vinyl chloride) thermal stabilizers, *J. Mater. Res. Technol.*, 2023, **24**, 3804–3814.
4 X. Ji, L. Ge, C. Liu, Z. Tang, Y. Xiao, W. Chen, Z. Lei, W. Gao, B. Sara, D. De, B. Shi, X. Zeng, N. Kong, X. Zhang and W. Tao, Capturing functional two-dimensional nanosheets from sandwich-structure vermiculite for cancer theranostics, *Nat. Commun.*, 2021, **12**, 1124–1141.
5 D. C. Nguyen, T. T. Bui, Y. B. Cho and Y. S. Kim, Preparation of a highly porous clay-based absorbent for hazard spillage mitigation *via* two-step expansion of vermiculite, *Minerals*, 2021, **11**(12), 1371.
6 L. A. Perez-Maqueda, C. Maqueda, J. L. Perez-Rodriguez, J. Subrt, Z. Cerny and V. Balek, Thermal behaviour of ground and unground acid leached vermiculite, *J. Therm. Anal. Calorim.*, 2012, **107**(2), 431–438.
7 Q. Wang, L. Yan, S. Yuan, Z. Wang and F. Yu, Vermiculite reshaped nickel-based hydrotalcite derived composites efficiently drive methane dry reforming, *J. Mater. Chem. A*, 2025, **13**, 2120–2133.
8 S. S. Salih, M. A. Shihab, H. N. Mohammed, M. Kadhom, N. Albayat and T. K. Ghosh, Chitosan-vermiculite composite adsorbent: Preparation, characterization, and competitive adsorption of Cu (II) and Cd (II) ions, *J. Water Process Eng.*, 2024, **59**, 105044.
9 J. L. Perez-Rodriguez, C. Maqueda, N. Murafa, J. Šubrt, V. Balek, P. Pulišová and A. Lančok, Study of ground and unground leached vermiculite II. Thermal behaviour of

ground acid-treated vermiculite, *Appl. Clay Sci.*, 2011, **51**(3), 274.

10 B. Liu, J. He, K. Huang, S. Feng, Z. Wang, X. Wu and B. Huang, Organic expanded vermiculite as an alternative to filler for improving aging resistance of asphalt mixture, *Case Stud. Constr. Mater.*, 2024, **20**, e03307.

11 X. Wang, J. Feng, J. Huang, T. Dai, S. Liu, Z. Wu, W. Mo and X. Su, Hydrothermal synthesis of a novel expanded VMT/xonotlite composite for thermal insulation, *Constr. Build. Mater.*, 2023, **367**, 130254.

12 O. Gencel, A. Sarı, A. Ustaoglu, G. Hekimoglu, E. Erdogmus, A. Yaras, M. Sutcu and V. V. Cay, Eco-friendly building materials containing micronized expanded vermiculite and phase change material for solar based thermo-regulation applications, *Constr. Build. Mater.*, 2021, **3**(1), 1–10.

13 P. R. K. Soda, K. Chakravarthi and K. M. Mini, Experimental and statistical investigation on strength and microcracks remediation in cement mortar using expanded vermiculite as a bacterial carrier, *J. Build. Eng.*, 2023, **63**, 105567.

14 H. Suquet, S. Chevalier, C. Marcilly and D. Barthomeuf, Preparation of porous materials by chemical activation of the Llano VMT, *Clay Miner.*, 1991, **26**(1), 49–60.

15 F. Olaosebikan, C. Dodds, G. Dimitrakis and S. Kingman, Continuous energy efficient exfoliation of vermiculite through microwave heating. International Journal of Mineral Processing, *Int. J. Miner. Process.*, 2012, **114**, 69.

16 R. R. Petersen, M. B. Olesen, J. König and Y. Yue, Expansion and shrinkage of lightweight vermiculite material at high temperatures, *Ceram. Int.*, 2023, **49**(14), 23605–23611.

17 W. Tian, Z. Li, Z. Ge, D. Xu and K. Zhang, Self-assembly of vermiculite-polymer composite films with improved mechanical and gas barrier properties, *Appl. Clay Sci.*, 2019, **180**, 105198.

18 R. Chai, X. Sun, S. An, T. Lin, H. Wang, W. Chen and Y. Song, Effect of VMT on in-situ super-stable mineralization and amelioration on sodic soil, *Environ. Technol. Inno.*, 2025, **38**, 104156.

19 R. R. Petersen, J. F. S. Christensen, N. T. Jørgensen, S. Gustafson, L. A. Lindbjerg and Y. Yue, Preparation and thermal properties of commercial VMT bonded with potassium silicate, *Thermochim. Acta*, 2021, **699**, 178926.

20 P. Zang, J. Tang, H. Zhang, X. Wang, L. Cui, J. Chen, P. Zhao and Y. Dong, Two-dimensional interfacial enhanced CO_2 adsorption performance of porous organic amine solids: Structure-activity relationships and DFT calculations, *Chem. Eng. J.*, 2024, **485**, 149938.

21 F. Dai, Q. Zhuang, G. Huang, H. Deng and X. Zhang, Infrared spectrum characteristics and quantification of OH groups in coal, *ACS Omega*, 2023, **8**(19), 17064.

22 F. Ding, T. Shen, S. Mao, X. Jin and M. Gao, Adsorption behavior and wettability alteration of bis-imidazolium salts on VMT: Experimental and theoretical studies, *Petrol. Sci.*, 2022, **19**(5), 2460.

23 J. Feng, M. Liu, L. Fu, S. Ma, J. Yang, W. Mo and X. Su, Study on the influence mechanism of Mg^{2+} modification on VMT thermal expansion based on molecular dynamics simulation, *Ceram. Int.*, 2020, **46**(5), 6413.

24 X. Huo, L. Wu, L. Liao, Z. Xia and L. Wang, The effect of interlayer cations on the expansion of VMT, *Mater. Sci. Forum*, 2015, **820**, 36–39.

25 Y. Xu, F. Ye, B. Xiong and C. Demartino, Mortar with natural light-weight expanded vermiculite aggregate: Physical and mechanical properties, *Constr. Build. Mater.*, 2024, **440**, 137226.

26 D. Dubey, A. S. Mirhakimi and M. A. Elbestawi, Negative Thermal Expansion Metamaterials: A Review of Design, Fabrication, and Applications, *J. Manuf. Mater. Process.*, 2024, **8**(1), 40.

27 J. Xu, Y. Xiao, J. Zhang, Z. Shang, Z. Tian, X. Zhu, K. Li and Y. Liu, Microwave expansion pretreatment for enhancing microwave-assisted alkaline extraction of hemicellulose from bagasse, *Biomass Convers. Biorefin.*, 2024, **14**, 9399–9406.

28 A. P. Yadav, A. K. Pandey, M. Samykano, B. Kalidasan and Z. Said, A review of organic phase change materials and their adaptation for thermal energy storage, *Inter. Mater. Rev.*, 2024, **69**(8), 380.

29 J. L. Perez-Rodriguez, M. L. Franquelo and A. Duran, TG, DTA and X-ray thermodiffraction study of wall paintings from the fifteenth century, *J. Therm. Anal. Calorim.*, 2020, **143**(4), 1–9.

30 C. Marcos and I. Rodriguez, Structural changes on vermiculite treated with methanol and ethanol and subsequent microwave irradiation, *Appl. Clay Sci.*, 2016, **123**, 304–314.